The Astrophysical Journal, 734:106 (9pp), 2011 June 20 doi:10.1088/0004-637X/734/2/106

PROTON ACCELERATION AT OBLIQUE SHOCKS

V. L. Galinsky and V. I. Shevchenko
ECE Department, UC San Diego, MC 407, La Jolla, CA 92093-0407, USA; vit@ucsd.edu
Received 2010 December 15; accepted 2011 April 6; published 2011 June 2

ABSTRACT

Acceleration at the shock waves propagating oblique to the magnetic field is studied using a recently developed theoretical/numerical model. The model assumes that resonant hydromagnetic wave–particle interaction is the most important physical mechanism relevant to motion and acceleration of particles as well as to excitation and damping of waves. The treatment of plasma and waves is self-consistent and time dependent. The model uses conservation laws and resonance conditions to find where waves will be generated or damped, and hence particles will be pitch-angle-scattered. The total distribution is included in the model and neither introduction of separate population of seed particles nor some ad hoc escape rate of accelerated particles is needed. Results of the study show agreement with diffusive shock acceleration models in the prediction of power spectra for accelerated particles in the upstream region. However, they also reveal the presence of spectral break in the high-energy part of the spectra. The role of the second-order *Fermi*-like acceleration at the initial stage of the acceleration is discussed. The test case used in the paper is based on ISEE-3 data collected for the shock of 1978 November 12.

Key words: acceleration of particles – methods: numerical – shock waves

Online-only material: color figures

1. INTRODUCTION

The idea of diffusive shock acceleration (DSA) at quasi-parallel shocks (Krymskii 1977; Axford et al. 1977; Bell 1978a, 1978b; Blandford & Ostriker 1978) based on the first-order *Fermi* mechanism of acceleration of charged particles by clouds of Alfvén waves excited on both sides of a shock wave was successful in explaining the main characteristics of accelerated particles. Following the work of Skilling (1975) and Bell (1978a, 1978b), Lee (1983; see also Gordon et al. 1999) developed the quasi-linear model that describes self-consistently the ion acceleration and the wave excitation at interplanetary shocks. It was assumed in Lee (1983) and Gordon et al. (1999) that some flux of protons (seed population) is injected at the shock front into the upstream plasma, and the dynamics of only this population due to interaction with waves was studied. As a result of cyclotron instability (Sagdeev & Shafranov 1961), Alfvén waves are excited, which scatter some particles toward the downstream region, creating the conditions for the first-order *Fermi* mechanism. Similar to Skilling (1975) and Bell (1978a, 1978b), it was assumed as well that the particle pitch-angle scattering due to cyclotron interaction is the fastest process, thus they always have an almost isotropic distribution function. The pitch-angle-averaged distribution function is a solution of the so-called convection-diffusion equation with right-hand side describing the ion source term (see, e.g., Equation (2.1) in Malkov & O'C Drury 2001). It was assumed that the flux density of the seed particles in the source term could be found by using results of the shock observations.

Although DSA-based analytical and numerical models (Lee 1983; Gordon et al. 1999; Zank et al. 2000; Li et al. 2003) were able to successfully explain many important features of the acceleration process, for example, power spectra of accelerated particles, dependence of accelerated particles on the distance from the shock front, and many others, there are important questions that stay open for a long time. Some very detailed analyses of the expectations of DSA models to observations of solar energetic particle events have been recently presented in Verkhoglyadova et al. (2009). Particularly, the predictions of the simpler steady-state models often do not agree with the results of time-dependent models (Rice et al. 2003; Li et al. 2003) that include time-dependent effects, such as, for example, balancing the shock dynamical timescale and the particle acceleration timescale to estimate maximum energies, the variability of the propagating shock, the influence of these factors on the self-excited wave field, and particle escape and propagation (see review by Zank et al. 2007).

It was discussed long ago that the thermal plasma can be considered as a source of the accelerated protons, and there was considerable evidence from observations (see, e.g., Tsurutani & Lin 1985) and simulations that shocks can directly accelerate ambient thermal particles (see reviews by O'C Drury 1983; Jones & Ellison 1991; and references therein). Malkov & Völk (1995) have shown that the wave fields needed for proton acceleration can be excited by a beam of the downstream tail protons injected into the upstream region. Since the DSA-based theoretical models did not consider the thermal plasma dynamics, they could not, in principle, include this mechanism in the macroscopic acceleration picture and describe the process of proton acceleration from the thermal plasma. Another shortcoming of the DSA models: they do not include the back reaction of the accelerated particles on the shock wave that can limit the process of acceleration (although some models include cosmic ray pressure on the shock structure as, for example, in Florinski et al. 2009). And again, this shortcoming is connected with limitations of DSA approach that evaluates only the dynamics of the high energetic tail of proton distribution. Detailed discussions of DSA-based models can be found in reviews by, e.g., O'C Drury 1983, Jones & Ellison 1991, Malkov & O'C Drury 2001, and references therein.

A new theoretical/numerical macroscopic model of the proton acceleration at quasi-parallel shocks that automatically includes both the thermal plasma injection scenario and modification of the shock structure due to the reaction of the accelerated protons was proposed in Galinsky & Shevchenko (2007, hereafter referred to as Paper I). Similar to the

analytical consideration by Lee (1982) and Gordon et al. (1999), in Paper I a quasi-linear approach was used to describe the wave–particle approximation and it was also assumed that resonant wave–particle interaction is the fastest process of the problem.

However, there are important differences between the approach used in Lee (1982), Gordon et al. (1999), and the one used in Paper I. First, in Paper I, in contrast to Lee (1982) and Gordon et al. (1999), plasma protons were not divided into two classes (1) resonant protons and (2) thermal plasma, and evolution of the entire gyro-phase-averaged proton distribution function was analyzed. Stability of the velocity distribution in the total interval of possible parallel velocities $v_\parallel$ was investigated for each distance from the shock front at each time step. Using a quasi-linear approach, the energy exchange between particles and waves for each interval of resonant parallel velocities $\Delta v_\parallel$ was analyzed and new velocity distribution function at the interval $\Delta v_\parallel$ as well as the corresponding wave power spectrum was found. As a result, the dynamics of the entire proton distribution and the wave power spectrum was studied as a function of time at each distance from the shock front. It was shown for the first time in Paper I how the problem of the particles' acceleration from the thermal distribution can be in a natural way included in a macroscopic model of acceleration. Second, the model constructed in Paper I takes into account the pressure of accelerated protons that can decelerate the upstream flow of the solar wind and, thus, modify the shock wave structure.

Using this model, in Paper I the proton acceleration was studied in the case of the shock wave propagating parallel to the ambient magnetic field. Results of the study showed agreement with DSA models in the prediction of power spectra for accelerated particles in the upstream region. However, this study has also revealed the presence of spectral break in the high-energy part of the particle spectra. It was also found that in the downstream region close to the shock front, a strong diffusion over perpendicular energy of particles with small absolute values of parallel velocity $v_\parallel$ in the shock reference frame takes place. These particles were quite likely crossing the shock interface multiple times and interacting with Alfvén waves at cyclotron resonance conditions that are different for waves in upstream and downstream regions. As a result, particles were not only pitch-angle-scattered but energized as well, mainly in the perpendicular direction. This process can be used to explain the observations of diffuse proton population ahead of Earth's bow shock and thus provides a critical component of the injection problem inherent to which most DSA-like models, are currently being addressed by invoking the shock microstructure, in particular, by application of the cross-shock potential (Zank et al. 2001).

It should be mentioned that most DSA-based models silently ignore a very important problem inherently present in the quasi-linear treatment of the pitch-angle scattering process—the resonant gap or lack of waves in resonance with particles having parallel velocity around V_A. This may result in slow or even no diffusion of particles across a 90° angle (see, e.g., Tsurutani et al. 2000). Thus, the formation of isotropic pinch-angle-scattered particle distribution function (PDF) required for DSA to work may be impossible or very difficult. The approach presented here does not rely on the complete isotropicity of PDF and hence does not have this limitation. Indeed, multiple crossings of the shock interface are possible even when particles are pitch-angle-scattered in less than 90°.

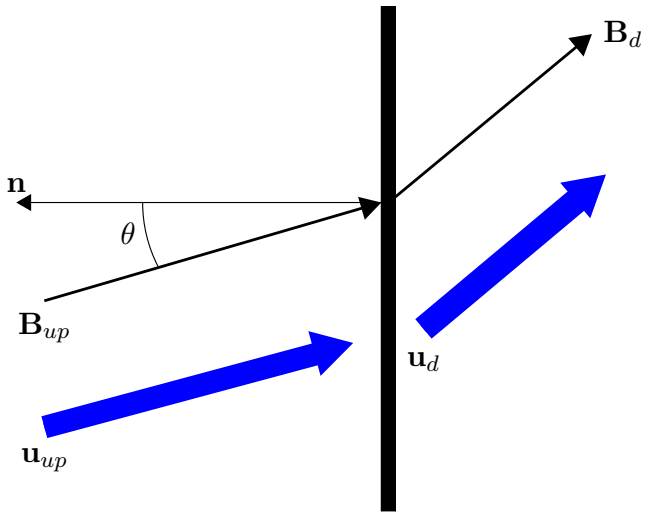

Figure 1. Oblique shock geometry in de Hoffmann–Teller frame.
(A color version of this figure is available in the online journal.)

In this paper, we will study the proton acceleration at a shock wave that propagates oblique to the interplanetary magnetic field.

2. EQUATIONS AND ALGORITHM FOR NUMERICAL SOLUTION

We consider a planar shock wave moving along the z-axis from the $+z$-direction obliquely to the magnetic field with angle θ between the magnetic field and the z-axis in the upstream region and will work in the wave front system of reference (a schematic drawing of the shock geometry is shown in Figure 1).

We assume that initially the shock front at $z = z_0$ divides the upstream and downstream plasmas with Maxwellian distributions with parameters that satisfy Rankine–Hugoniot boundary conditions (see, e.g., Jones & Ellison 1991):

$$
\begin{aligned}
&[\rho \mathbf{u}\cdot\hat{\mathbf{n}}]_{\rm d}^{\rm up} = 0,\\
&\left[\mathbf{u}\cdot\hat{\mathbf{n}}\left\{\frac{\gamma}{\gamma-1}P+\frac{1}{2}\rho u^2+\frac{B^2}{4\pi}\right\}-\frac{(\mathbf{B}\cdot\hat{\mathbf{n}})(\mathbf{B}\mathbf{u})}{4\pi}\right]_{\rm d}^{\rm up} = 0,\\
&[\rho\mathbf{u}(\mathbf{u}\cdot\hat{\mathbf{n}})+(P+B^2/8\pi)\hat{\mathbf{n}}-(\mathbf{B}\cdot\hat{\mathbf{n}})\mathbf{B}/4\pi]_{\rm d}^{\rm up} = 0, \qquad (1)\\
&[\mathbf{B}\cdot\hat{\mathbf{n}}]_{\rm d}^{\rm up} = 0,\\
&[\hat{\mathbf{n}}\times(\mathbf{u}\times\mathbf{B})]_{\rm d}^{\rm up} = 0.
\end{aligned}
$$

Here, ρ, $\mathbf{u}$, and P are zero, first, and second moments of the proton distribution function, $\hat{\mathbf{n}}$ is a unit vector in the direction of the shock normal (negative z-direction), $[f(z)]_{\rm d}^{\rm up}$ is the difference between initial upstream (up) and downstream (d) values of $f(z)$ at the wave front.

We would like to note that we need Rankine–Hugoniot conditions only at time $t = 0$, when isotropic particle distributions without wave fields are assumed both downstream and upstream, hence no anisotropic pressure terms or wave pressure contributions are required in Equation (1). Similar to Paper I, we solve the spatial-temporal problem of plasma–wave dynamics by considering the upstream and downstream plasmas as a single plasma with inhomogeneous parameters.

As in Lee (1983), Gordon et al. (1999), and in Paper I, we do not use any external forces and rely only on resonant wave–particle interaction self-consistently included in the

model to excite Alfvén waves and accelerate particles. We introduce the wave action

$$W^{\leftrightarrow}(t, z, \omega_k) = |B_k^{\leftrightarrow}|^2/8\pi\omega_k,$$

which describes the wave packets propagating parallel ($\rightarrow$) and anti-parallel ($\leftarrow$) to the external magnetic field in a medium with varying parameters that are calculated from the momentum of the PDF. $|B_k|^2$ is the spectral density of the wave magnetic field. The resonance conditions for interaction with such waves have the form

$$\omega_k - k v_\parallel \mp \omega_c = 0. \quad (2)$$

Here, ω_k and k are the frequency and wave number of Alfvén waves, respectively, and ω_c is the proton cyclotron frequency. The $\mp$signs in Equation (2) describe interactions with waves at normal and anomalous Doppler resonances, correspondingly. It should be mentioned that Equation (2) includes both the noncompressional mode (Alfvén waves) as well as the right-hand-polarized magnetosonic mode, and the term "Alfvén wave" is used in this paper for both of these modes.

Cyclotron resonant interaction leads to pitch-angle scattering of particles, so resonant protons interacting at both possible resonances (2) with each of the broadband packets' field $W^{\leftrightarrow}(t, z, \omega_k)$ diffuse along the lines (Vedenov et al. 1962; Rowlands et al. 1966; Kennel & Engelmann 1966)

$$w^{\leftrightarrow} = v_\perp^2 + (v_\parallel - v_{\rm ph}^{\leftrightarrow})^2 = \text{const.}, \quad (3)$$

where $v_{\rm ph}^{\rightarrow} = v_A$ and $v_{\rm ph}^{\leftarrow} = -v_A$.

As a result of resonance interaction, a shell-like distribution of protons $f = f(w)$ is formed in the interval of resonant velocities v_z.

As was discussed above, we will study the dynamics of the wave excitation and particle acceleration relying on the thermal plasma as a source of the so-called seed population that excites waves needed for particle acceleration. Thus, similar to Paper I, we will analyze the stability of the entire gyro-phase-averaged proton distribution function. By averaging the proton kinetic equation over a period of oscillations, we obtain in quasi-linear approximation the equation for the so-called background distribution function of protons $f(t, z, v_\parallel, v_\perp)$:

$$\frac{\partial f}{\partial t} + v_z \frac{\partial f}{\partial z} = QL_f(f, W^{\rightarrow}, W^{\leftarrow}). \quad (4)$$

Equations for wave actions in quasi-linear approximation have the form

$$\frac{\partial W^{\leftrightarrow}}{\partial t} + \frac{\partial}{\partial z}(v_{gz}^{\leftrightarrow} W^{\leftrightarrow}) = QL_W^{\leftrightarrow}(f, W^{\leftrightarrow}). \quad (5)$$

Here, $v_{gz}^{\leftrightarrow}$ is the z-component of the group velocity for waves propagating in parallel and anti-parallel directions.

Right-hand-side terms in Equations (4) and (5) are quasi-linear operators that in the case of a temporal problem have the following form in the plasma reference frame:

$$QL_f = \frac{2\pi e^2}{m_p^2 c^2} \sum_{\mp} \left\{ \hat{L}\left[v_\perp^2 \frac{\omega_k W_k^{\rightarrow}}{|v_\parallel - \partial\omega/\partial k|} \hat{L} f \right]\Big|_{v_\parallel = v_{\rm ph}^{\rightarrow}(\mp\omega_c + \omega)/\omega} + \hat{L}\left[v_\perp^2 \frac{\omega_k W_k^{\leftarrow}}{|v_\parallel + \partial\omega/\partial k|} \hat{L} f \right]\Big|_{v_\parallel = v_{\rm ph}^{\leftarrow}(\mp\omega_c + \omega)/\omega} \right\} \quad (4')$$

$$QL_W^{\leftrightarrow} = \frac{v_{\rm ph}^{\leftrightarrow}}{v_{\rm A}} \frac{\pi^2}{n_0} \frac{\omega_c^2}{\omega_k} W_k^{\leftrightarrow} \int v_\perp^3 \hat{L} f \, dv_\perp \Big|_{v_\parallel = v_{\rm ph}^{\leftrightarrow}(\mp\omega_c + \omega)/\omega} \quad (5')$$

$$\hat{L}\psi = \frac{\partial \psi}{\partial v_\parallel} + \frac{\omega_k - k_{||} v_{||}}{v_\perp k_{||}} \frac{\partial \psi}{\partial v_\perp}.$$

The sum in Equation (4′) takes into account interactions at normal and anomalous Doppler resonances. Thus, the quasi-linear term (4′) in the right-hand side of Equation (4) takes into account all four possible interactions with MHD waves propagating in both directions along the magnetic field. The "−" sign corresponds to normal Doppler resonance and "+" sign corresponds to anomalous resonance for wave packets propagating parallel ($\rightarrow$) and anti-parallel ($\leftarrow$) to the magnetic field. The spatial dependence of waves generated or damped due to any of these four resonance interactions will probably be rather complicated, but the above description should allow predicting not only the wave spectrum but also the wave helicity as a function of distance from the shock. It should be mentioned that even in the upstream region the wave polarizations "do not seem to be confirmed" by the DSA theories (Kennel et al. 1986).

Equations (4) and (5) describe the processes of wave excitation and particle acceleration in the system under consideration. Since these equations are non-stationary and non-homogeneous nonlinear equations, we solve them numerically. The region over z with size L where the processes of wave excitation and particle acceleration take place stretches in both directions from the shock front. The size L of the region is chosen to be much larger than the characteristic scale of the quasi-linear relaxation. We divide the region L into small intervals with locations

$$z_i, \; i = 1, 2, 3, \ldots N_z \quad (6)$$

and will solve Equations (4) and (5) at each interval for each time step. To do this, we introduce the wave spectrum with a wide band of possible wave numbers:

$$k_i, \; i = 0, 1, \ldots N_k \quad (7)$$

to assure resonant cyclotron interaction with protons that have any parallel velocity from the entire possible interval of resonant velocities $v_\parallel$ on their distribution function.

Similar to Paper I, scale-separation techniques will be used to numerically solve Equations (4) and (5) by assuming that characteristic temporal and spatial scales of pitch-angle diffusion (microscopic scales) are smaller than the time step and size of each spatial interval (macroscopic scales). This means that the steady state of the plasma–wave system is developed at each time step at any given distance from the shock front. The steady state at some interval of resonant velocities is settled in two cases: (1) when the pitch-angle-averaged distribution function is formed $\hat{L} f = 0$ or (2) when the resonant waves are totally absorbed $W_k = 0$ at the interval of resonant velocities being considered. Thus, at the end of each time step, the right-hand-side terms in Equations (4) and (5) are equal to zero.

For the purpose of calculating the input from the resonant particles to the waves and vice versa, we divide the entire region of possible parallel and perpendicular velocities into small intervals with grid locations

$$v_\parallel^i, \; i = 1, 2, 3, \ldots N_{v_\parallel} \quad (8)$$

$$v_\perp^i, \; i = 1, 2, 3, \ldots N_{v_\perp}. \quad (9)$$

To calculate the input from waves to resonant particles and vice versa, we need to find the free energy available in the particle distribution for each resonant velocity interval. The amount of free energy available in nth interval of resonant velocities $v_\parallel \in [v_\parallel^n - \delta v_\parallel, v_\parallel^n + \delta v_\parallel]$ is defined by the difference between the energy contained in the current PDF and the energy contained in the pitch-angle-scattered PDF, both taken over the resonance interval. We find the pitch-angle average function at each time step using conservation of proton number along diffusion lines (3) (see Paper I):

$$\langle f(t, z, v_\parallel, v_\perp)\rangle^{\leftrightarrow} = \frac{\int_{S_n^{\leftrightarrow}} f(t, z, w^{\leftrightarrow}, \alpha - \alpha')d\alpha'}{\int_{S_n^{\leftrightarrow}} d\alpha'}, \quad (10)$$

where the α coordinate is directed along lines $w^{\leftrightarrow} = \text{const}$. and $S_n^{\leftrightarrow}$ is the nth interval of resonant velocities for waves propagating parallel ($\rightarrow$) or anti-parallel ($\leftarrow$) to the external magnetic field $v_\parallel \in [v_\parallel^n - \delta v_\parallel, v_\parallel^n + \delta v_\parallel]$.

The amount of particle free energy for each resonance region is obtained as a variation of the proton kinetic energy in the final and initial states in a frame of reference where the bulk of the plasma is at rest:

$$\Delta F_m^{\leftrightarrow}(t, z) = \frac{m_p}{2}\int_{S_m^{\leftrightarrow}} [\langle f(t, z, v_\parallel, v_\perp)\rangle^{\leftrightarrow} - f(t, z, v_\parallel, v_\perp)] \times \{v_\perp^2 + [v_\parallel - u(t, z)]^2\}d\mathbf{v}, \quad (11)$$

where $u(t, z)$ is the bulk plasma velocity.

We calculate the balance of energy between waves and particles for each resonance interval as

$$\Delta E_n^{\leftrightarrow}(t, z) = \sum_{k\in\{n\}} E^{\leftrightarrow}(t, z, \omega_k) - \Delta F_n^{\leftrightarrow}. \quad (12)$$

Here, $\Delta E_n^{\leftrightarrow}(t, z)$ is the change of the wave energy density in the nth resonance region and $\{n\}$ represents all harmonics belonging to the nth resonant interval that can be found from the resonance condition (2). The first term in the right-hand side of Equation (12) is the total wave energy density in the nth resonance region at the previous time step, with the quantity $E^{\leftrightarrow}(t, z, \omega_k)$ defined by

$$E^{\leftrightarrow}(t, z, \omega_k) = -W_k^{\leftrightarrow}\frac{\partial D}{\partial \omega_k}\frac{\omega_k^2}{k^2c^2} \quad (13)$$

$$D(\omega_k, k) = k^2c^2 + \omega_{pp}^2\frac{\omega_k}{\omega_k - \omega_{cp}} + \omega_{pe}^2\frac{\omega_k}{\omega_k + \omega_{ce}}, \quad (14)$$

where $E^{\leftrightarrow}(t, z, \omega_k)$ is the sum of the potential and kinetic energy densities of the wave with frequency ω_k that is defined from the equation

$$D(\omega_k, k) = 0. \quad (14')$$

In our case, the potential and kinetic wave energy densities are equal to each other and $E^{\leftrightarrow}(t, z, \omega_k) = |B_k^{\leftrightarrow}|^2/4\pi$.

The algorithm for numerical solutions of Equations (4) and (5) can be described by the following procedure.

1. In accordance with the assumption that the steady state of the plasma–wave system is developed at each time step at any given distance from the shock front, we update the distribution function as well as the wave spectrum at the beginning of each time step by integrating Equations (4) and (5) with zero right-hand sides. We obtain the new distribution function at every $z \times v_\parallel \times v_\perp$ grid location by using flux conservation and assuming one-dimensional streaming of plasma in force-free environment. The waves are updated for every z_i by using conservation of their action in streaming medium with locally varying parameters.
2. The new distribution function is used to find the proton density, temperature, as well as the local rest frame of reference for every z_i. Using these parameters, we calculate the pitch-angle diffusion lines (Equation (3)).
3. By using Equation (10), we obtain the pitch-angle-scattered distribution function in every resonant region $v_\parallel \in [v_\parallel^n - \delta v_\parallel, v_\parallel^n + \delta v_\parallel]$.
4. After that, using Equation (11), we check if the energy of the particles is increased or decreased, that is if the distribution function is stable or unstable with respect to wave generation in the current resonance interval.
   (a) If it is unstable, we use the pitch-angle-scattered PDF as a new one for the current resonance interval. We assign the available energy to the waves in this interval by using Equation (12) and proceed to the next resonant interval.
   (b) If the PDF is stable but waves are present in the current resonant region, the waves will interact with the particles and transfer some or all of their energy. The new PDF and the new wave level in the resonant region are found by using the same Equations (10)–(12).
5. Since the levels of the newly found PDF can be different in adjacent resonant intervals this locally stable PDF does not yet represent the global wave–particle equilibrium state. In order to find this global state we use an aggregation procedure, that is, we combine adjacent resonant intervals where the PDF has been pitch-angle-scattered and use Equation (10) to find the common pitch-angle-scattered PDF. We then repeat the entire procedure (4–5) iteratively until we arrive at the (quasi)-stationary partitioning of energy between waves and particles.

In the case when initially there are waves in the plasma, we should first perform procedure 4(b) by using Equations (10)–(12) and then proceed after that with the solution of equations at the first time step using the above described numerical algorithm for the solution.

We should stress that the state with the (quasi)-stationary partitioning of energy between waves and particles (mentioned in item 5) is not a stationary state of the whole system of Equations (4) and (5). The isolation of this state in our numerical procedure merely represents the fact that the particle pitch-angle scattering due to cyclotron interaction is the fastest process, hence, the partitioning of wave–particle energy looks quasi-stationary in comparison with all other processes, including differential streaming of particles.

3. RESULTS OF SOLUTION

To show that protons are accelerated from the thermal core and that the waves needed for their acceleration are excited due to cyclotron instability (Sagdeev & Shafranov 1961), we assume that initially there is no seed population and no waves in the system.

As was discussed before, we integrate the system of Equations (4) and (5) for the case of oblique shock. We work in the shock front reference frame and postulate that the upstream and downstream plasmas are Maxwellian with temperatures that

are related by Rankine–Hugoniot boundary conditions (1). The dimensionless equations that are employed to update the distribution function and the wave spectrum at the beginning of each time step (procedure 1 of *the algorithm*) have the form

$$\frac{\partial f}{\partial t} + v_z \frac{\partial f}{\partial z} = 0 \tag{15}$$

$$\frac{\partial W^{\leftrightarrow}}{\partial t} \pm \cos\theta \frac{\partial}{\partial z}\left(\frac{v_A}{v_{A1}} W^{\leftrightarrow}\right) = 0. \tag{16}$$

And the energy balance Equation (12) can be written as

$$\Delta\widetilde{B}_n^{\leftrightarrow 2}(t,z) = \widetilde{B}_n^{\leftrightarrow 2}(t,z) - \pi\beta_{\rm up}\int_{S_n^{\leftrightarrow}} [\langle f(t,z,v_\parallel,v_\perp)\rangle^{\leftrightarrow} - f(t,z,v_\parallel,v_\perp)] \times \left\{v_\perp^2 + [v_\parallel - u(t,z)]^2\right\} v_\perp dv_\perp dv_\parallel. \tag{17}$$

Here, $\beta_{\rm up} = v_{\rm Tup}^2/v_{\rm Aup}^2$, $v_{\rm Tup}$, and $v_{\rm Aup}$ are the initial values of the gas kinetic-to-magnetic pressure ratio, the proton thermal velocity, and Alfvén speed in the upstream region correspondingly. $\Delta\widetilde{B}_n^{\leftrightarrow 2}$ in Equation (17) represents the change of the dimensionless wave magnetic energy density in nth resonance region (see Equation (12)).

In obtaining Equations (15)–(17), we introduced dimensionless magnetic variance

$$\widetilde{B}_{\rm dls}^2 = \widetilde{B}^2/B_0^2, \tag{18}$$

where $\widetilde{B}^2 = \sum |B_k|^2$

and used a normalized PDF

$$f_{\rm dls}(t,z,v_\parallel,v_\perp) = \frac{v_{Tp}^3}{n_{\rm up}} f(t,z,v_\parallel,v_\perp). \tag{19}$$

We also introduced dimensionless velocity, length, and time

$$\mathbf{v}_{\rm dls} = \frac{\mathbf{v}}{v_{Tp}}, \quad t_{\rm dls} = \frac{t}{t_0}, \quad z_{\rm dls} = \frac{z}{z_0}. \tag{20}$$

Here, z_0 and t_0 are macroscopic length and time, respectively, connected by the relation $z_0 = v_{\rm Tup}t_0$.

We omitted the subscript "*dls*" in Equations (15)–(17).

To cover the possible interval of accelerated energies up to several MeV per nucleon, we choose the value of maximal velocity of protons as $v_{\parallel\,\max} = 10^3$. The size of the parallel velocity interval was chosen as $\Delta v_\parallel = 0.25$.

We used the following grid dimensions in the numerical solution of Equations (4) and (5):

$$N_z = 100, \quad N_{v_\parallel} = 4000, \quad N_{v_\perp} = 100, \tag{21}$$

and the number of harmonics in this study was $N_k = 10^6$.

We studied the case of an oblique shock from 1978 November 11 and 12. The particle and wave observations for this event were described in detail (see Kennel et al. 1984; Tsurutani et al. 1983). The parameters of the solar wind plasma measured during the observations were

$$B_0 = 6.85nT, \quad u_{\rm up} = 2.4\times 10^7 {\rm cm\,s^{-1}}, \quad n_{\rm up} = 4\,{\rm cm^{-3}}.$$

All plasma parameters have been chosen to match the observed values so as to generate a shock wave propagating obliquely to the magnetic field at the angle $\theta = 41^\circ$ with the shock compression value equal to $r = u_{\rm up}/u_{\rm d} = 3.3$. No initial wave activity has been introduced either upstream or downstream of the shock and waves were self-consistently generated by the model itself.

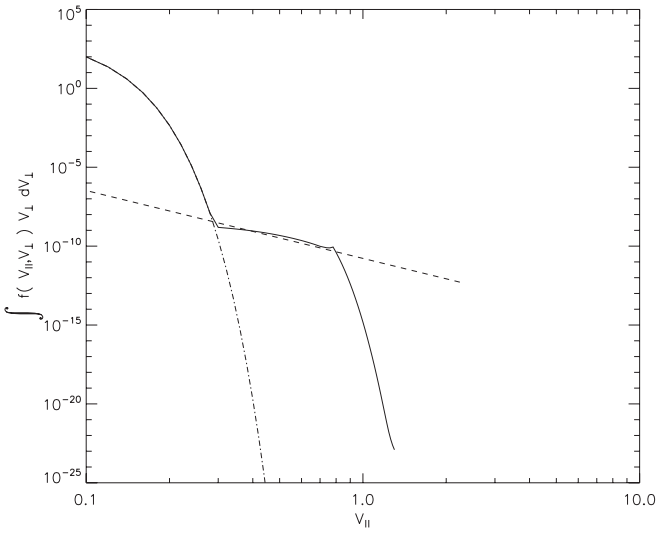

Figure 2. Snapshot of the proton distribution function integrated over the perpendicular velocity $\int f(t,z,v_\parallel,v_\perp)v_\perp dv_\perp$ typical for spatial/temporal area in the upstream region close to the shock front. The dashed line is the line $v_\parallel^{-\beta}$. (Looking at this plot one should avoid mistakenly assuming that it contradicts the first principles. Indeed, the particle number is not conserved—the total area under the solid line (the late-time distribution) is greater than the area under the dot-dashed curve. But the figure shows only a small local part of the time-dependent PDF, hence the particle number is not required to be conserved.)

One of the main results obtained in this study is the spectrum of the accelerated protons as a function of the parallel velocity shown in Figure 2 by using log–log scale. One can see a power-like spectrum of protons with the exponent close to $\beta = 4.3$ that is related to the compression value $\beta = 3r/(r-1)$. This result is in agreement with that of the DSA-based theory (see, e.g., Gordon et al. 1999). However, solution of quasi-linear equations in the frame of our model has shown that there is a break on the spectrum at large parallel velocity.

Since the whole distribution function of protons is analyzed in our model, we can find out how the initial profiles of density and velocity change due to the wave excitation and particle acceleration. Simulation results for the density and velocity profiles and wave magnetic field amplitude are shown in the two top panels of Figure 3. For comparison the initial profiles of the density and velocity are displayed as well by dotted lines with the front initial position at $z = 0.33$. One can see that the shock profiles do not change significantly with time.

The very interesting result obtained in this simulation is the distribution of the intensity of waves excited in the process of the proton acceleration (see the bottom panel in Figure 3). It can be seen clearly that the wave intensity is much higher in the downstream region with maximal intensity at the shock front itself. Although waves are mainly excited in the upstream region, they are convected by streaming plasma ($u_{\rm up} \gg V_A$) to the shock front, and greatly amplify the wave intensity at the front and in the downstream region. The amount of wave field amplification due to this convection depends on the shock parameters and may result in the development of a highly nonlinear region with $\widetilde{B}/B_0 \gg 1$. The quasi-linear approach in this case can give, of course, only qualitatively correct results. We would like to emphasize that this large-amplitude wave field at the

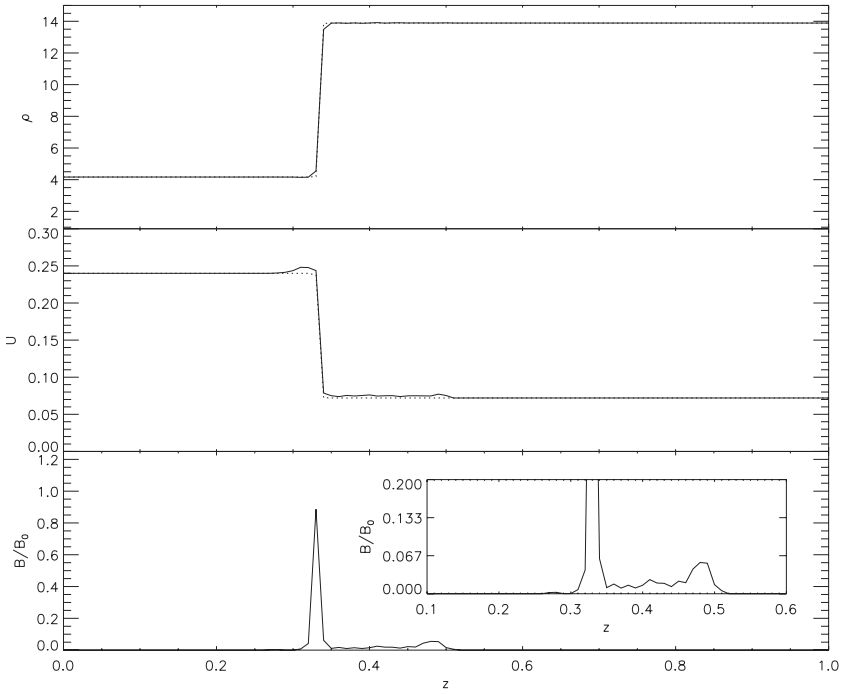

Figure 3. Profiles of density, bulk velocity, and wave amplitude (from top to bottom, ordinate units are arbitrary, z is in units of $2 \times 10^6 r_B$, where r_B is the proton gyroradius). In the first two panels, the solid lines show calculated profiles and the dotted lines correspond to the initial shock discontinuity.

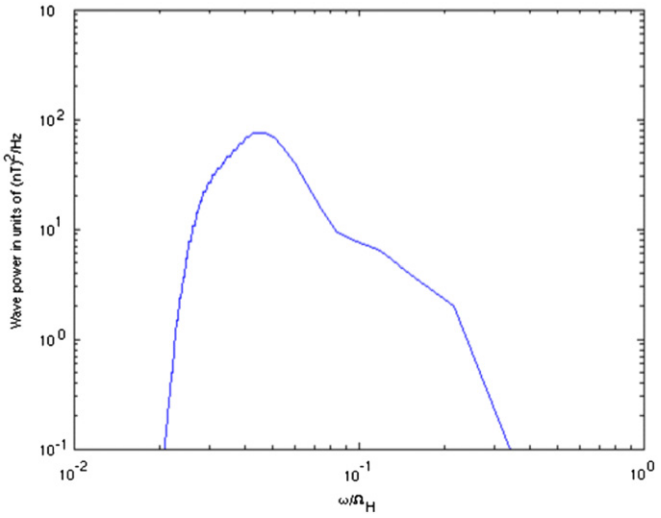

Figure 4. Upstream wave spectra near the shock.
(A color version of this figure is available in the online journal.)

shock interface does not necessarily preclude the applicability of the quasi-linear approach as the quasi-linear treatment is only indirectly responsible for its development. We should also emphasize that the energy balance approach used for integration of Equations (4) and (5) or Equations (15) and (16) is based on a simple assumption that the wave–particle system relaxes to the equilibrium state (that is to the state where there are no energy exchanges between waves and particles). The quasi-linear formalism is not required for derivation of the energy balance method. And hence the method can be applied even for large-amplitude monochromatic wave regimes (similar to the waves used in the acceleration model by Sugiyama & Terasawa 1999 where quasi-linear approach is not applicable).

The power spectrum of the excited waves in the upstream region close to the shock front is shown in Figure 4. The spectral density has a maximum at the frequency around 0.1 Ω_H with a drop of wave power at lower and higher frequencies.

In Figure 5, a set of contour plots of the proton distribution function in the downstream region in close vicinity of the shock front is shown. One can see that in addition to pitch-angle diffusion, the particles in some intervals of the parallel velocity are energized mainly in the perpendicular direction.

4. DISCUSSION

In this model a quasi-linear approach is used inside each resonant interval so the points on the parallel velocity grid inside each resonant interval should be close enough to each other to reach the overlapping of the trapping regions of neighboring harmonics and to make the quasi-linear approach applicable. The condition on the distance over $v_\parallel$ between two neighboring points (two neighboring harmonics) has the form

$$\delta v_\parallel < \{\Omega_{cp} k v_\perp\}^{1/2}/k, \tag{22}$$

where $\Omega_{cp} = e\widetilde{B}/mc$, $\widetilde{B} = (|B_k|^2\,\delta k)^{1/2}$ is a root-mean-square magnetic field of the wave harmonic, $v_\perp \approx v_T$ is the characteristic perpendicular velocity, $\delta v_\parallel$, δk are the distances between the neighboring harmonics over the parallel velocity and the wave number, respectively, and $|B_k|^2$ is the spectral energy density of the electromagnetic fluctuations.

By using cyclotron resonance condition it follows that

$$\delta v_\parallel < \left(\frac{e^2\,|B_k|^2}{m^2c^2}\frac{v_T^2}{\omega_c}\right)^{1/3}. \tag{23}$$

The width of each resonant interval should satisfy the condition

$$\Delta v_\parallel \gg \delta v_\parallel. \tag{24}$$

We checked that conditions (23) and (24) were satisfied in our study.

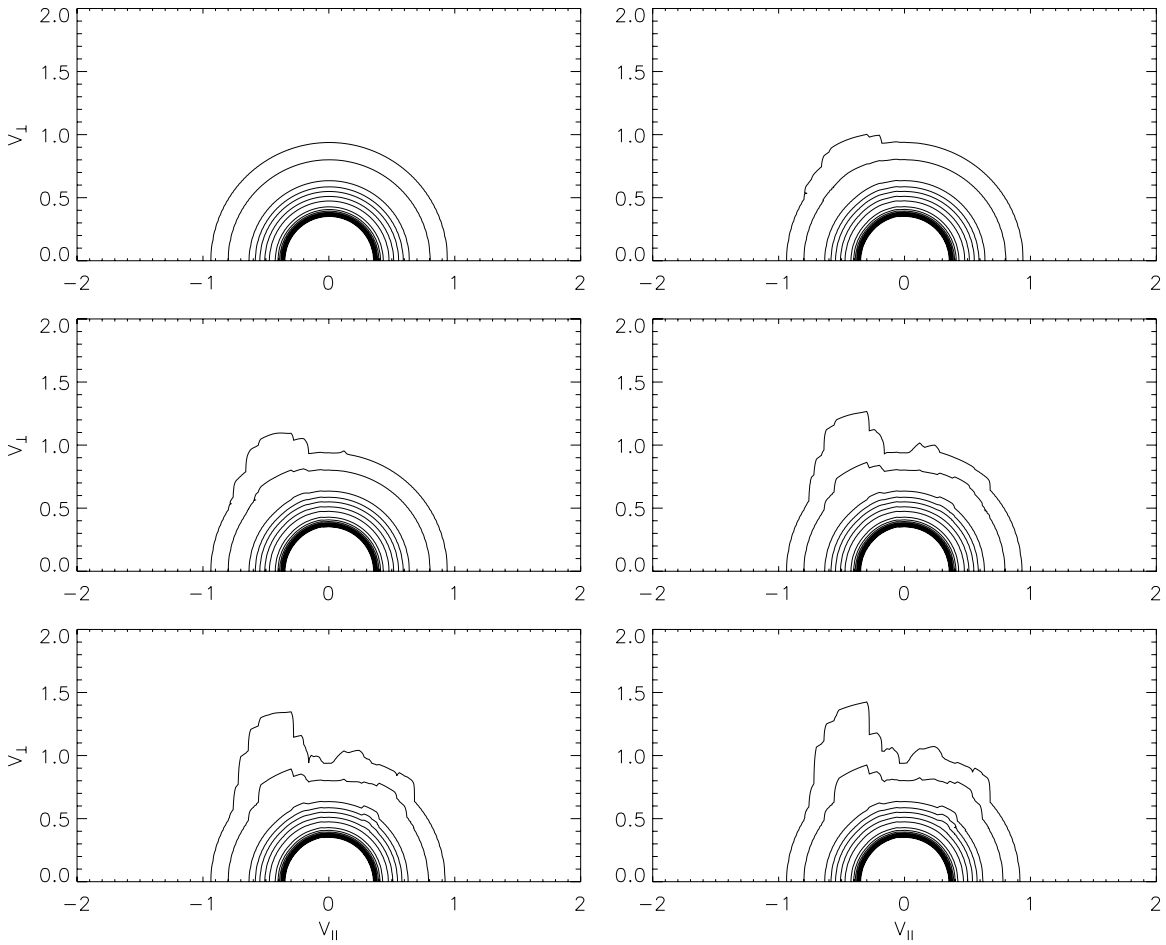

Figure 5. Time sequence of contour plots ($v_{\parallel} - v_{\perp}$) in the downstream region in close vicinity of the shock front (from left to right, then from top to bottom).

Our model does not restrict itself by following only the energetic particles and takes into consideration the thermal particles as well, so it permits us to find out how the shock is modified due to the acceleration process. We would like to note that we consider a collisionless plasma and do not include any nonresonant instabilities in the model. Although nonresonant fire-hose instability may be responsible for initial shock formation, the results of numerical simulations suggest (Quest 1988) that it is not important for containment of already established shocks. The shock wave can be formed in collisionless plasma only due to the collective mechanism of dissipation (see Sagdeev 1966). The density and velocity profiles shown in Figure 3 demonstrate the high efficiency of collisionless dissipation by resonance cyclotron interaction in supporting the initially created upstream–downstream asymmetry and in keeping the shock wave almost intact.

Another interesting feature that the model revealed is the presence of spectral break in the high-energy part of the particles power spectrum. The possible explanation of the origin of the break may lie in the non-stationary nature of the model. We found that the position of the break depends both on distance from the shock front and on time elapsed since the acceleration process has started. As acceleration to higher energies requires more time it is not clear yet if an asymptotic stationary solution without the break can be reached in a finite time for any shock configuration or, on the contrary, if the position of the break will stabilize at some point in time.

The solution obtained above demonstrated that neither seed population nor initial waves was needed for the acceleration process to start. We would like to note once more that all previous DSA-based macroscopic models needed a seed population for the description of the acceleration process at the shocks. There was an understanding that the "seed" population is injected from the thermal background (see, e.g., O'C Drury 1983; Jones & Ellison 1991). Malkov & Völk (1995) have revealed that the tail protons from the downstream thermal distribution penetrating into the upstream region and exciting waves needed for particle acceleration are just this seed population. However, this

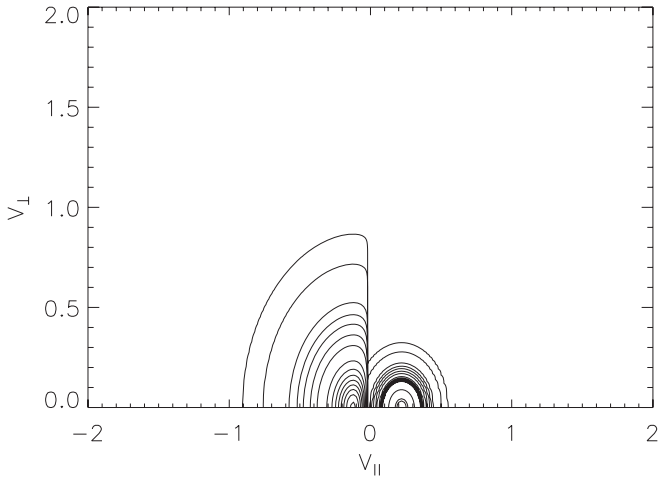

Figure 6. Updated distribution function at the beginning of the first time step in the upstream region close to the shock front.

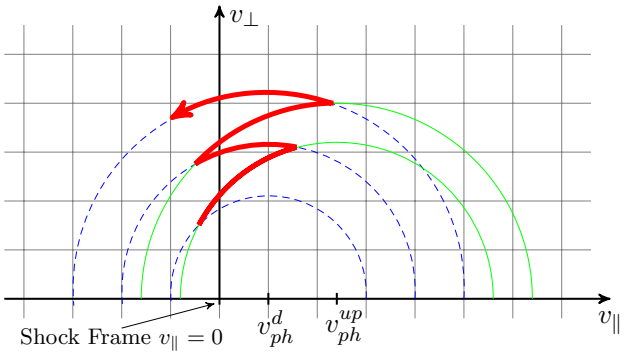

Figure 7. Ions interacting with waves in the upstream region (phase speed $v_{\rm ph}^{\rm up}$) move along the solid circles. After crossing the shock front to the downstream region, interaction with downstream waves (phase speed $v_{\rm ph}^{d}$) makes them move along the dashed circles. If ions change the parallel velocity to a negative value (i.e., directed upstream) as they interact with downstream waves, they can return to the shock front and escape to the upstream region (Sugiyama & Terasawa 1999).

(A color version of this figure is available in the online journal.)

mechanism, studied in local approximation by Malkov & Völk (1995), could not be included, in principle, in DSA-based macroscopic models because they are limited by consideration of energetic particles only. We would like to note that the Malkov–Völk mechanism is automatically incorporated in our macroscopic model. In Figure 6, the updated distribution function of protons (see procedure 1 of the *algorithm*) in the upstream region close to the wave front is shown at the beginning of the first time step. This is just the plasma-beam distribution with the beam component formed by the tail particles of the downstream distribution that crossed the shock front. This distribution is unstable with respect to the excitation of MHD waves that is needed for the resonant particles to change their velocities. As a result, some particles can cross the shock front once more and eventually be accelerated.

Detailed analysis of the proton distribution function in the downstream region presented in Figure 5 has shown that the proton energization takes place at the values of the negative parallel velocities close to the shock speed. As was discussed before, protons with negative velocities larger than the shock velocity can escape the downstream region. The energizing mechanism is similar to the one proposed by Sugiyama & Terasawa (1999) to explain the acceleration of particles when a monochromatic Alfvén wave of large amplitude exists at the shock front. In this mechanism protons with this "boundary" parallel velocity can cross the shock several times. Due to resonant interaction with waves excited in upstream and downstream plasmas they move over diffusion lines that are different since the phase velocities (Alfvén speed) are different in these plasmas (see Figure 7). As a result of such a motion, protons are not only pitch-angle-scattered but energized as well mainly in the perpendicular direction.

We compared the wave spectrum obtained in this study with observations and with results of the DSA model (Gordon et al. 1999). To do this we used the following relations between the frequency and wave number and corresponding power densities (see Gordon et al. 1999):

$$2\pi\, f = \mathbf{kV}_{sw} = kV_{sw}\cos 25^\circ$$

$$P_f df = 2B_k^2 dk,$$

where the factor of two arises because the frequency f includes both signs of the wave number k.

In Figure 8, the observed frequency spectrum (Kennel et al. 1986) as well as two spectra—(1) calculated by using our model and (2) obtained by Gordon et al. (1999)—are shown. It is possible to say that the wave power density spectrum obtained here shows more reasonable agreement with observations than DSA results.

It should be mentioned that we also found qualitative agreement of our model with the results of the first statistical

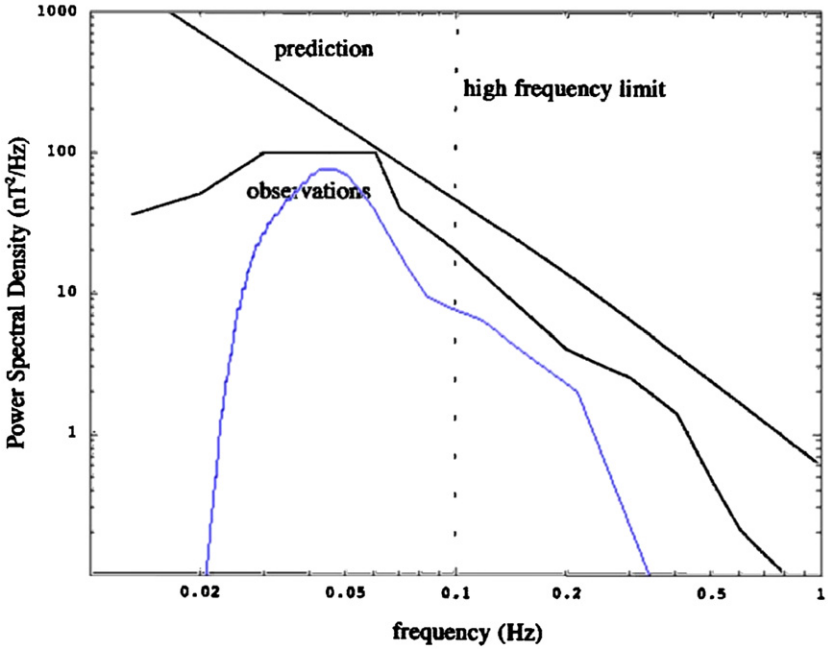

Figure 8. Upstream wave spectra near the shock. The upper two lines are theoretical predictions of Gordon et al. (1999) and the results of the analysis of ISEE-3 data from Kennel et al. (1986; 0.1 Hz frequency in spacecraft frame corresponds to 10^{-1} ω/Ω_H in solar wind frame).

(A color version of this figure is available in the online journal.)

observational study on shock acceleration of particles (Tsurutani & Lin 1985). Based on the strength or speed of the shock we were able to identify several distinct signatures of behavior of accelerated particles in the shock vicinity. Sharp intensity spikes at the shock or slow rise of upstream ion fluxes has been spotted in different ranges of shock parameters. Of course, quantitative comparison will require more detailed study across wide range of shock parameters and will be reported elsewhere.

We would like to note that we limited ourselves in this study by considering only resonant wave–particle interactions similar to DSA-based models. Including a nonresonant interaction is a challenging problem. We defer the discussion of possible effects of this interaction to a subsequent paper.

Another unsolved problem in the study of shock acceleration mechanism is the role of nonlinear wave–wave interactions in the upstream region. We studied a parametric interaction of Alfvén and acoustic waves that led to the development of nonlinear structures by using the so-called derivative nonlinear Schrödinger (DNLS)-type equation (Shevchenko et al. 2002). In particular, it was shown (Shevchenko et al. 2003) that nonlinear interaction can lead to the development of short large-amplitude magnetic structures (SLAMSs) that were observed in the solar wind by Schwartz et al. (1992). Such nonlinear wave structures can reflect protons (see, e.g., Claßen & Mann 1998) and thus add to the energy that goes to downstream heating and wave excitation. Our approach permits us to include the wave–wave interaction in the model of the shock acceleration. We will consider these questions in detail elsewhere.

The authors are grateful to Martin Lee and Gary Zank for useful critical remarks and suggestions. The NASA grant NNX09AG95G is acknowledged for support of this study.

REFERENCES

Axford, W. I., Leer, E., & Skadron, G. 1977, Proc. 15th ICRC (Plovdiv), 11, 132
Bell, A. R. 1978a, MNRAS, 182, 147
Bell, A. R. 1978b, MNRAS, 182, 443
Blandford, R. D., & Ostriker, J. P. 1978, ApJ, 221, L29
Claßen, H., & Mann, G. 1998, A&A, 330, 381
Florinski, V., Decker, R. B., le Roux, J. A., & Zank, G. P. 2009, Geophys. Res. Lett., 36, 12101
Galinsky, V. L., & Shevchenko, V. I. 2007, ApJ, 669, L109
Gordon, B. E., Lee, M. A., Möbius, E., & Trattner, K. J. 1999, J. Geophys. Res., 104, 28263
Jones, F. C., & Ellison, D. C. 1991, Space Sci. Rev., 58, 259
Kennel, C. F., Coroniti, F. V., Scarf, F. L., Livesey, W. A., Russell, C. T., & Smith, E. J. 1986, J. Geophys. Res., 91, 11917
Kennel, C. F., & Engelmann, F. 1966, Phys. Fluids, 9, 2377
Kennel, C. F., et al. 1984, J. Geophys. Res., 89, 5419
Krymskii, G. F. 1977, Dokl. Akad. Nauk SSSR, 234, 1306
Lee, M. A. 1982, J. Geophys. Res., 87, 5063
Lee, M. A. 1983, J. Geophys. Res., 88, 6109
Li, G., Zank, G. P., & Rice, W. K. M. 2003, J. Geophys. Res. (Space Phys.), 108, 1082
Malkov, M. A., & O'C Drury, L. 2001, Rep. Prog. Phys., 64, 429
Malkov, M. A., & Völk, H. J. 1995, A&A, 300, 605
O'C Drury, L. 1983, Rep. Prog. Phys., 46, 973
Quest, K. B. 1988, J. Geophys. Res., 93, 9649
Rice, W. K. M., Zank, G. P., & Li, G. 2003, J. Geophys. Res. (Space Phys.), 108, 1369
Rowlands, J., Shapiro, V. D., & Shevchenko, V. I. 1966, Sov. J. Exp. Theor. Phys., 23, 651
Sagdeev, R. Z. 1966, in Reviews of Plasma Physics, Vol. 4, ed. M. A. Leontovich (New York: Consultants Bureau), 23
Sagdeev, R. Z., & Shafranov, V. D. 1961, Sov. J. Exp. Theor. Phys., 12, 130
Schwartz, S. J., Burgess, D., Wilkinson, W. P., Kessel, R. L., Dunlop, M., & Luehr, H. 1992, J. Geophys. Res., 97, 4209
Shevchenko, V. I., Galinsky, V. L., & Ride, S. K. 2002, J. Geophys. Res. (Space Phys.), 107, 1367
Shevchenko, V. I., Sagdeev, R. Z., Galinsky, V. L., & Medvedev, M. V. 2003, Plasma Phys. Rep., 29, 545
Skilling, J. 1975, MNRAS, 172, 557
Sugiyama, T., & Terasawa, T. 1999, Adv. Space Res., 24, 73
Tsurutani, B. T., & Lin, R. P. 1985, J. Geophys. Res., 90, 1
Tsurutani, B. T., Smith, E. J., & Jones, D. E. 1983, J. Geophys. Res., 88, 5645
Tsurutani, B. T., Zhang, L. D., Mason, G. S., Lakhina, G. S., Hada, T., Arballo, J. K., & Zwickl, R. D. 2000, in AIP Conf. Proc. 528, Acceleration and Transport of Energetic Particles Observed in the Heliosphere, ed. R. A. Mewaldt et al. (Melville, NY: AIP), 165
Vedenov, A. A., Velikhov, E. P., & Sagdeev, R. Z. 1962, Nucl. Fusion Suppl., Part 2, 465
Verkhoglyadova, O. P., Li, G., Zank, G. P., Hu, Q., & Mewaldt, R. A. 2009, ApJ, 693, 894
Zank, G. P., Li, G., & Verkhoglyadova, O. 2007, Space Sci. Rev., 130, 255
Zank, G. P., Rice, W. K. M., Le Roux, J. A., Cairns, I. H., & Webb, G. M. 2001, Phys. Plasmas, 8, 4560
Zank, G. P., Rice, W. K. M., & Wu, C. C. 2000, J. Geophys. Res., 105, 25079